Available online at www.sciencedirect.com
SCIENCE DIRECT®
ELSEVIER
Journal of Petroleum Science and Engineering 39 (2003) 231–246
JOURNAL OF PETROLEUM SCIENCE & ENGINEERING
www.elsevier.com/locate/jpetscieng

Prediction of wettability variation and its impact on flow using pore- to reservoir-scale simulations

Matthew D. Jackson*, Per H. Valvatne, Martin J. Blunt

Department of Earth Science and Engineering, Centre for Petroleum Studies, Imperial College, London SW7 2AZ, UK

Received 5 May 2002; received in revised form 27 September 2002

Abstract

We describe a pore- to reservoir-scale investigation of wettability variation and its impact on waterflooding. We use a three-dimensional pore-scale network model of a Berea sandstone to predict relative permeability and capillary pressure hysteresis. We successfully predict experimentally measured relative permeability data for the water-wet case, and demonstrate that the model captures experimentally observed trends in waterflood recovery for mixed-wet media. We then focus upon the effect of variations in initial water saturation associated with capillary rise above the oil–water contact (OWC). This may lead to wettability variations with height because the number of pore-walls which may be rendered oil-wet during primary drainage, increases as the oil saturation increases. We investigate empirical hysteresis models in which scanning curves are used to connect bounding drainage and waterflood curves for a given initial water saturation, and find that if wettability varies with initial water saturation, then the scanning water relative permeability curves predicted by the empirical model are significantly higher than those predicted by the network model. We then use a conventional simulator, in conjunction with the relative permeability curves obtained from the network and empirical models, to investigate the reservoir-scale impact of wettability variations on waterflooding. If the wettability varies with height above the OWC, we find that using the network model to generate scanning relative permeability curves yields a significantly higher recovery than using empirical models or assuming that the reservoir is uniformly oil-wet or water-wet. This is because the scanning water curves are generally low (characteristic of water-wet media), yet the residual oil saturation is also low (characteristic of oil-wet media). Our aim is to demonstrate that network models of real rocks may be used as a tool to predict wettability variations and their impact on field-scale flow.

Keywords: Pore-scale; Network model; Wettability; Transition zone; Reservoir-scale

1. Introduction

The wettability of a crude oil/brine/rock system can have a significant impact on flow during oil recovery, and upon the volume and distribution of the residual oil (Craig, 1971; Owens and Archer, 1971; Salathiel, 1973; Morrow et al., 1986; Anderson, 1987; Morrow, 1990; Jadhunandan and Morrow, 1995). Wettability depends on the mineralogy of the rock, the composition of the oil and water, the initial water saturation, and the temperature (Buckley et al., 1989; Buckley, 1995; Buckley and Liu, 1998;

* Corresponding author. Tel.: +44-20-7594-6538; fax: +44-20-7594-7444.
E-mail address: mattjack@ic.ac.uk (M.D. Jackson).

0920-4105/03/$ - see front matter © 2003 Elsevier Science B.V. All rights reserved.
doi:10.1016/S0920-4105(03)00065-2

Dubey and Waxman, 1991; Dubey and Doe, 1993; Wolcott et al., 1993). Several studies have successfully used network models to investigate the effect of wettability variations on flow at the pore-scale (Mohanty and Salter, 1983; Heiba et al., 1983; Kovscek et al., 1993; McDougall and Sorbie, 1995; Blunt, 1997a,b, 1998; Dixit et al., 1997, 1998, 1999; Hui and Blunt, 2000). These models have progressively captured more of the physics of pore-scale displacement mechanisms; however, until recently, there has been less focus on capturing the complex pore-scale topology of a typical reservoir rock. Consequently, although these models have successfully interpreted phenomenon observed experimentally, they have not been truly predictive.

The aim of this study is to investigate and predict the effect of wettability variations on flow at the reservoir-scale, using a pore-scale network model in conjunction with reservoir-scale conventional simulations. We use a three-dimensional (3-D) network model, which combines a physically based pore-scale model of wettability alteration (Blunt, 1998) with a network representation of a Berea sandstone (Bakke and Øren, 1997; Øren et al., 1998; Øren and Bakke, 2002). The network is reconstructed directly from a sample of the sandstone, so the pore-size distribution and coordination number are fixed and are not tuned to match experimental data. This makes the model more likely to be truly predictive, although it should be emphasized that predictive modelling of relative permeability for all types of rock and for all wettabilities is a long way off (Blunt et al., 2002). Nevertheless, we successfully predict experimental relative permeability data for water-wet Berea sandstone (Oak, 1990), as well as waterflood recoveries for mixed-wet Berea (Jadhunandan and Morrow, 1995). We match the mixed-wet data reasonably well even when we assume that wettability variations result only from variations in the initial water saturation following primary drainage. This causes wettability variations because the number of pore-walls rendered oil-wet increases as the initial water saturation decreases.

In many reservoirs, wettability changes as a function of height above the OWC (Jerauld, 1996a,b; Jerauld and Rathmell, 1997; Hamon, 2000). We reproduce this trend using network modelling, again assuming that the wettability variations are caused only by changes in initial water saturation. We compare the predictions of relative permeability from network modelling with results from empirical hysteresis models that use scanning curves to connect bounding drainage and waterflood curves for a given initial water saturation (Killough, 1976; Carlson, 1981). The scanning water relative permeability curves predicted by the empirical model are considerably higher than those predicted by the network model. When the network model-derived relative permeabilities are used in a reservoir-scale simulation of waterflooding above the oil/water contact, they lead to higher oil recoveries than simulations using empirical models. This demonstrates that pore-scale wettability changes have an impact on field-scale flow and oil recovery.

2. The network model

The 3-D network model is a cube of volume 27 mm^3, containing 12,349 pores and 26,146 throats, reconstructed directly from a sample of Berea sandstone (Bakke and Øren, 1997; Øren et al., 1998) (Fig. 1). Each pore and throat is represented as a duct with a square, circular or triangular cross-section, characterized by an inscribed radius which controls the threshold capillary entry pressure, effective corner angles which control the amount of fluid held in wetting layers, and an effective volume which controls the mobile (non-clay bound) saturation (Blunt, 1997a,b, 1998; Zhou et al., 1997; Øren et al., 1998; Firincioglu et al., 1999; Patzek, 2001). Empirical formulae are used to compute the hydraulic conductance of each pore and throat (Zhou et al., 1997). The absolute permeability of the network is 2600 mD and the pore and throat inscribed radii range from 0.9 to 73 μm. Two-phase flow is simulated for primary drainage and waterflooding, assuming that capillary forces dominate, so the pores and throats are filled in order of increasing capillary entry pressure. This is reasonable for low capillary number flow (Hilfer and Øren, 1996; Blunt, 1997a).

The drainage cycle begins with the network fully saturated with water and strongly water-wet, with the receding contact angle $\theta_r = 0°$. Oil then enters the network, and as the capillary pressure is increased step by step, invades the pore or throat with the

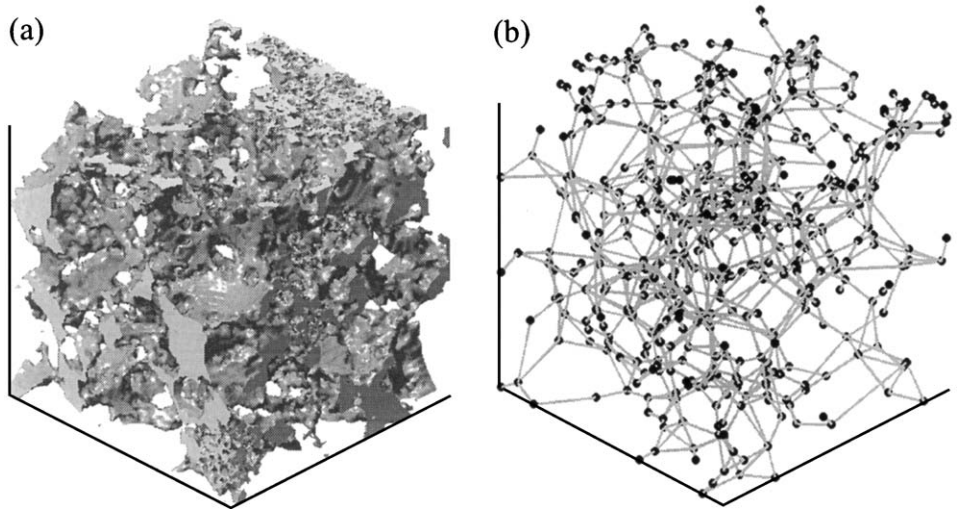

Fig. 1. (a) Reconstructed pore space at a resolution of 3 μm from Øren et al. (1998). Each side of the cube measures 3 mm. (b) The corresponding network that honors the topology of the pore space.

lowest capillary entry pressure in an invasion percolation process (Wilkinson and Williamsen, 1983; Dias and Wilkinson, 1986). Capillary entry pressures are calculated using the approach of Øren et al. (1998). At each step, water and oil saturations, relative permeabilities, and the capillary pressure are calculated subject to pressure boundary conditions at the inlet and outlet faces, and periodic boundaries on the other faces. To avoid end-effects, only a subset of the network model is included. Drainage is complete when a target capillary pressure or saturation has been reached or when all pores and throats have been invaded by oil.

Wettability variations are modelled by changing the advancing contact angle, θ_a, assigned to each oil-filled pore (Blunt, 1997b, 1998). Different pores and throats may have different contact angles. Depending upon the number of pores and throats invaded by oil, and the range of advancing contact angles, this approach allows us to model a mixed wet system, in which only those pores invaded by oil become oil-wet, a fractionally wet system, in which a fraction of the pores and throats invaded by oil become oil-wet, and a system which remains water-wet.

Water injection is then simulated. There are three distinct types of water invasion: piston type, pore-body filling, and snap-off. The capillary entry pressures for piston type and snap-off processes are calculated using the approach of Øren et al. (1998). The capillary entry pressure for pore-body filling is given by a parametric model (Blunt, 1998):

$$P_{\mathrm{cap}} = \frac{2\gamma\cos\theta_a}{r} - \gamma\sum_{i=1}^{n} A_i x_i \qquad (1)$$

where n is the number of surrounding throats filled with oil, r is the pore radius, x_i are random numbers between 0 and 1, and A_i are arbitrary parameters. Pore-body filling is a cooperative process (Lenormand and Zarcone, 1984; Lenormand et al., 1988) favoured when n is small (many surrounding throats contain water) and suppressed for large n (few surrounding throats filled with water). Eq. (1) accounts for the effect of converging/diverging pore geometries that can lead to negative values of P_{cap} even for $\theta_a < 90°$ (Blunt, 1998). In this paper, the weighting parameters were chosen to be $A_1 = 0$, $A_2 = A_3 = A_4 = A_5 = 0.03$ μm^{-1}. For comparison, Blunt (1998) used values of $A_1 = A_2 = A_3 = A_4 = A_5 = 0.015$ μm^{-1}. These values are broadly consistent with those derived for pores in a regular rectangular lattice (Lenormand and Zarcone, 1984). Small changes in these parameters have little impact on the relative permeabilities and residual oil saturations, particularly for water-wet systems.

Piston-like advance leaves the centre of the pore or throat filled with water, but if the advancing contact

angle is large enough, water also remains in the crevices with a layer of oil sandwiched in-between. Oil can flow through these layers (Salathiel, 1973; Zhou et al., 1997), which are stable until the two oil/water interfaces meet (Blunt, 1998).

During water injection, water and oil saturations, relative permeabilities, and the capillary pressure, are calculated in the same way as for drainage. Injection is complete when a target capillary pressure or saturation has been reached or when all available pores and throats have been invaded by water.

3. Predicting experimental data using the network model

We begin by comparing the network model predictions with experimental data from water-wet Berea cores (Oak, 1990). The oil and water viscosities used in the experiments were 1.40 and 1.05 cP, respectively, and the interfacial tension was 30 mN m^{-1}. During drainage, the receding contact angle is assumed to be 0°; there are no other parameters to adjust. Fig. 2 shows the match: it is good whether plotted on linear (Fig. 2a) or logarithmic (Fig. 2b) axis, although there is a slight tendency to overestimate the oil relative permeability at low water saturations. To predict the imbibition data, we assumed a uniform distribution of contact angles and adjusted the minimum and maximum values to obtain a match. The best match, shown in Fig. 3, was obtained using advancing contact angles drawn at random from a uniform distribution with a minimum of 50° and a maximum of 80°. Again, the match is good for both the water and oil relative permeabilities, whether plotted on linear (Fig. 3a) or logarithmic (Fig. 3b) axis.

Given that the Oak (1990) data was obtained from water-wet cores, it is perhaps surprising that the advancing contact angles which best match the data are quite large. However, it should be remembered that contact angles measured at a smooth flat surface may not resemble those found within the pore space of a typical reservoir rock, because of the additional complexities introduced by converging and diverging pore and throat geometries, surface roughness, and heterogeneous mineralogy (e.g. Hirasaki, 1991; Buckley et al., 1996; Zhou et al., 2000). As yet, there are no experimental techniques available to measure contact angles in real porous media. Consequently, it is not easy to relate contact angles measured at a smooth flat surface to those used in a network model, and at present, it is probably most suitable to consider the angles used in a network model as effective properties which can be adjusted to match experimental data for a given rock specimen and wettability and which take into account the

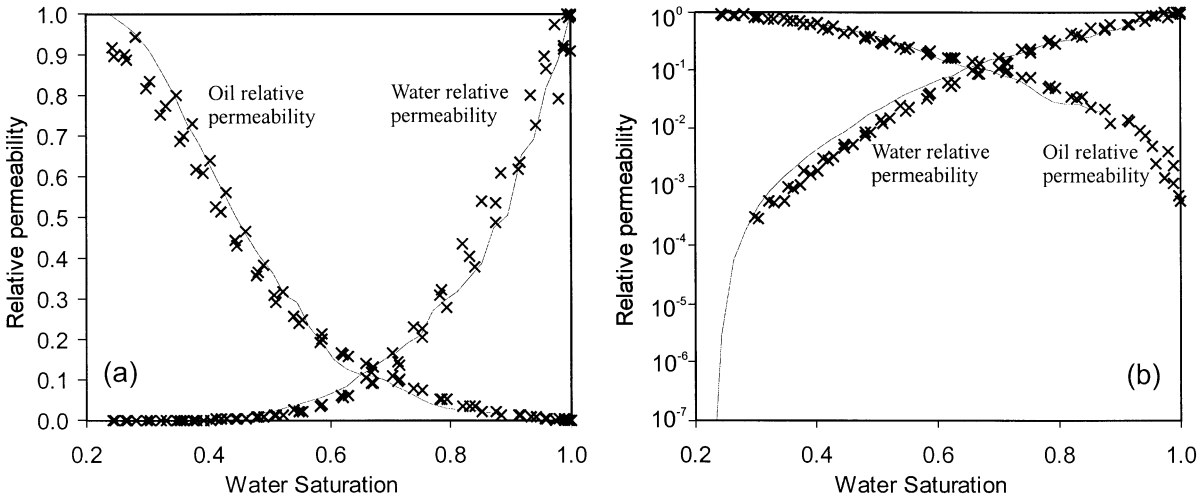

Fig. 2. Drainage relative permeability predicted from the network model (lines) and measured on a water-wet Berea core (crosses; data from Oak (1990)). Plotted on linear scale in (a) and on logarithmic scale in (b).

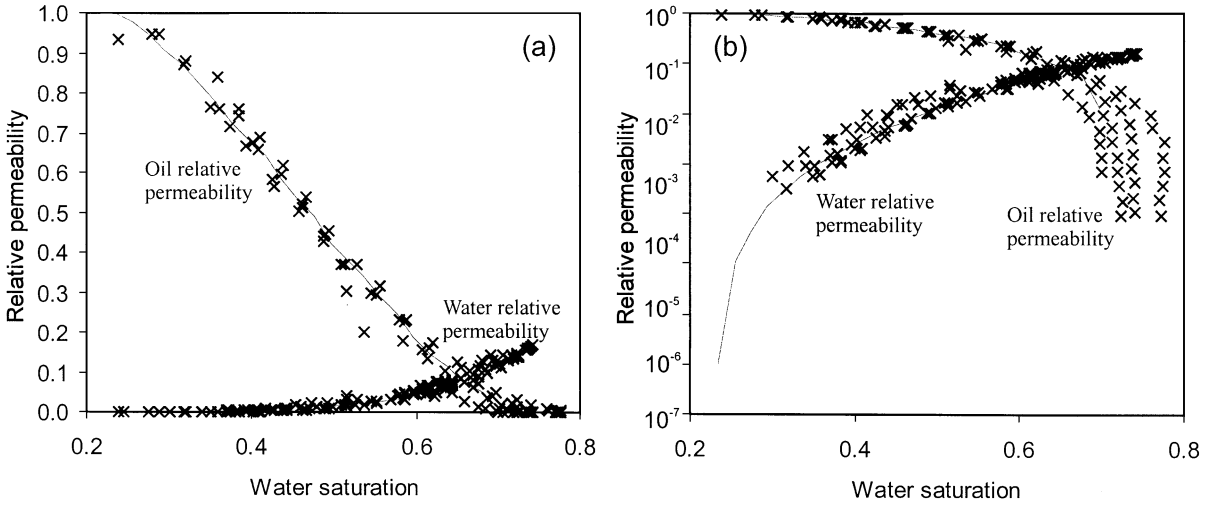

Fig. 3. Waterflood (imbibition) relative permeability predicted from the network model (lines) and measured on a water-wet Berea core (crosses; data from Oak (1990)). Plotted on linear scale in (a) and on logarithmic scale in (b).

complexities found within the pore space of the rock (e.g. Dixit et al., 1997).

Jadhunandan and Morrow (1995) performed an exhaustive study of the effects of wettability on waterflood recovery from Berea sandstone, and we now compare the network model predictions with some of their experimental data. They waterflooded core samples that had been aged at different temperatures in different crude oils and brines, with different initial water saturations. Our hypothesis is that, for a given crude oil, brine and reservoir (or core) conditions, the distribution of contact angles in pores occupied by oil is similar regardless of the initial water saturation (S_{wi}). Wettability variations are caused principally by variations in S_{wi} because the number of pore-walls rendered oil-wet following primary drainage increases as S_{wi} decreases (Jerauld, 1996a,b; Jerauld and Rathmell, 1997; Hamon, 2000). This hypothesis enables us to use data from a system at one value of S_{wi} to predict wettability trends in a reservoir with varying S_{wi}; for example, associated with a transition zone above the OWC. Our assumption of a fixed distribution of contact angles for pores contacted by oil is not necessarily correct; for low S_{wi}, the initial capillary pressure is larger than for high S_{wi}. This will tend to favour the collapse of wetting films, making the pores invaded by oil more oil-wet (Kovscek et al., 1993). Furthermore, curvature effects may tend to make the smaller oil-filled pores more oil-wet (Kovscek et al., 1993) which would also result in the distribution of contact angles becoming more oil-wet as S_{wi} decreases.

We used the network model to match experimental waterflood data from one crude oil/brine system and aging temperature, where S_{wi} was varied from 7.8% (yielding the most oil-wet cores) to 31.1% (yielding the most water-wet cores; see Fig. 7 in Jadhunandan and Morrow (1995)). To reach the lowest S_{wi} of 7.8% during primary drainage, we adjusted the clay content of our network model. We then simulated primary drainage to the different values of S_{wi}, followed by wettability alteration and then waterflooding. The network model predicted relative permeability curves and we used these in a semi-analytic Buckley–Leverett analysis, ignoring capillary pressure, to predict waterflood recovery. The matching parameter was the distribution of advancing oil/water contact angles. We assumed that the contact angle distribution after wettability alteration in pores and throats invaded by oil was uniform between 180° and some lower limit. This reduced the match to a single parameter. Fig. 4 shows predicted and experimental results when the contact angle distribution varied uniformly between 110° and 180°. This is a plausible range based on the limited

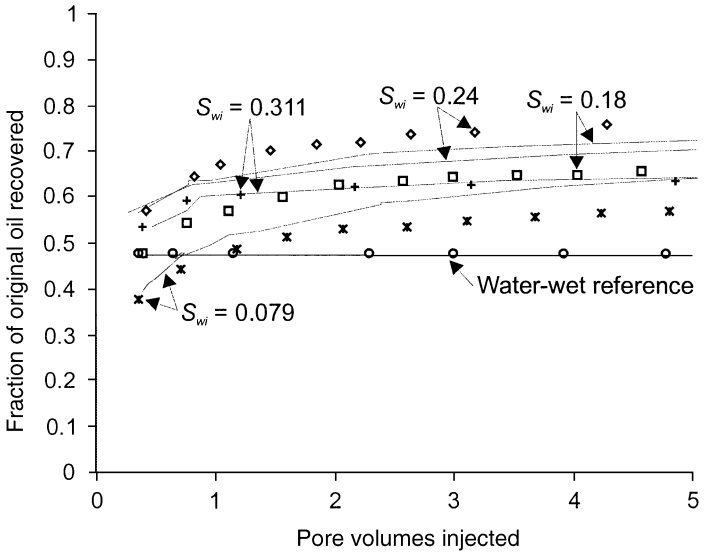

Fig. 4. Predictions of oil recovery (solid lines) using pore-scale modeling compared with experimental results from Jadhunandan and Morrow (1995) (points). In the network model we assumed that the pores contacted by oil had a uniform distribution of contact angles assigned at random in the range 110–180°, regardless of the initial water saturation S_{wi}. The water-wet reference case was simulated assuming a uniform distribution of contact angles from 35° to 85°.

experimental data available for contact angles on flat surfaces where the crude oil induces an appreciable change (Buckley et al., 1989, 1996; Hazlett, 1990; Onda et al., 1996). The reference 'water-wet' case (a core flood without wettability alteration) was simulated assuming a uniform contact angle distribution in the range 35–85°. This is similar to the distribution used to match the Oak (1990) data shown in Fig. 3.

The agreement between experiment and prediction is good, bearing in mind that a single adjustable parameter was used to predict four recovery curves. The significant feature is that the trend in recovery is correctly predicted: the water-wet case gives maximum recovery at breakthrough, but there is significant trapping of oil. With wettability alteration, recovery is higher with significant production of oil post-breakthrough. The most favourable recovery is found for an intermediate value of S_{wi} of around 20%, and is lower for higher and lower values of S_{wi}. This qualitative trend in recovery has been discussed previously in network modelling studies (Blunt, 1998; Dixit et al., 1999). However, there are two differences with this work. First, we attempt a quantitative match with experiment. Second, hitherto, the trend has been modelled in a network by keeping S_{wi} constant and changing the distribution of contact angles. In this study, we keep the distribution of contact angles constant and vary S_{wi}.

The pore-scale explanation for the results is as follows. For low values of S_{wi}, waterflooding is essentially a primary drainage type displacement, since almost all the pores and throats are oil-wet (i.e. non-wetting to water). The water fills the larger pores and has a high relative permeability, resulting in rapid breakthrough. Recovery continues after breakthrough due to the drainage of oil through layers, but this is a very slow process. As S_{wi} increases, pore-level displacement can be initiated from pores and throats already filled with water. This leads to a more connected advance, as pores with a more favourable capillary entry pressure (essentially with the lowest contact angles) are filled first. This gives a delayed breakthrough and more favourable waterflood recoveries. For much larger values of S_{wi}, recovery drops. This is because appreciable quantities of oil can be trapped: the large number of completely water-filled water-wet pores prevents the escape through oil layers of oil surrounded by water.

There are some significant differences between prediction and experiment and we tend to underestimate the impact of varying S_{wi} on waterflood recovery. It is possible to improve the match by allowing the distribution of contact angles to be different for different values of S_{wi}. Fig. 5 shows these results. The range of contact angles is from 130° to 180° for $S_{wi}=0.24$ and from 85° to 180° for $S_{wi}=0.18$. The other cases are not adjusted. The agreement is now good in all cases, except that we over-predict recovery at later times for the lowest value of S_{wi}. The predicted results for this case are relatively insensitive to the contact angle distribution and so it is not easy to improve the match significantly.

The Berea network that we have used in the modelling studies has a larger permeability than the cores used by Jadhunandan and Morrow (1995). Also, while the experimental results were generally reproducible, similar cores with similar values of S_{wi} gave recoveries that varied by 0.1 or more, within the range of mismatch of our predictions. Further work is planned to tune the distribution of contact angles to match the Amott indices and then predict waterflood recovery, enabling, in theory, relative permeabilities as a function of S_{wi} to be predicted from a single wettability measurement.

The conclusion of this section is that it is possible to predict waterflood recovery for different values of S_{wi} in mixed-wet systems within the range of experimental variation. We can now use the network model with some confidence to predict recovery in a reservoir with a wettability trend associated with a transition zone above the oil/water contact. This will be the subject of the following sections.

4. Relative permeability hysteresis

Relative permeability curves typically exhibit hysteresis during drainage and waterflooding, and several workers have argued that this can have a significant impact on flow during recovery (Land, 1968; Killough, 1976; Carlson, 1981; Kossack, 2000). Killough (1976) and Carlson (1981) presented empirical models for hysteresis in which relative permeabilities can vary between drainage and waterflood via intermediate scanning curves (Fig. 6). The drainage and waterflood curves, which bound the scanning curves, are determined experimentally, and

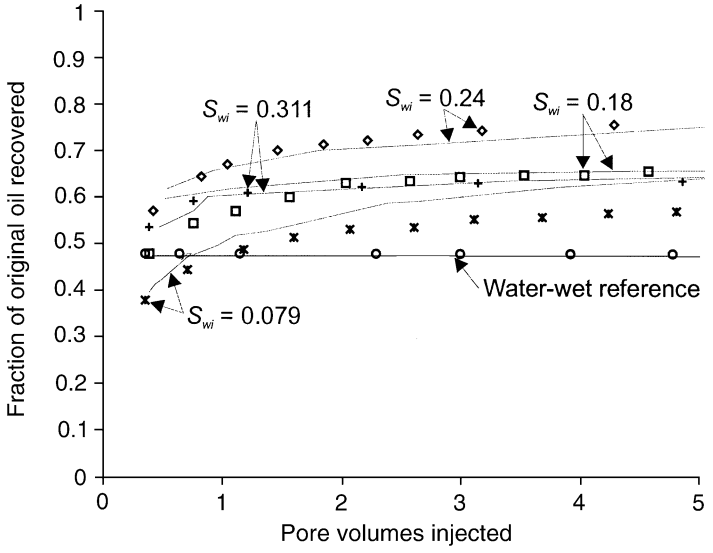

Fig. 5. Predictions of oil recovery (solid lines) using pore-scale modeling compared with experimental results from Jadhunandan and Morrow (1995) (points). In the network model we assumed that the pores contacted by oil had a uniform distribution of contact angles assigned at random in the range 110–180°, for $S_{wi}=0.311$ and $S_{wi}=0.079$. The range of contact angles is 130–180° for $S_{wi}=0.24$ and 85–180° for $S_{wi}=0.18$. The water-wet reference case was simulated assuming a uniform distribution of contact angles from 35° to 85°.

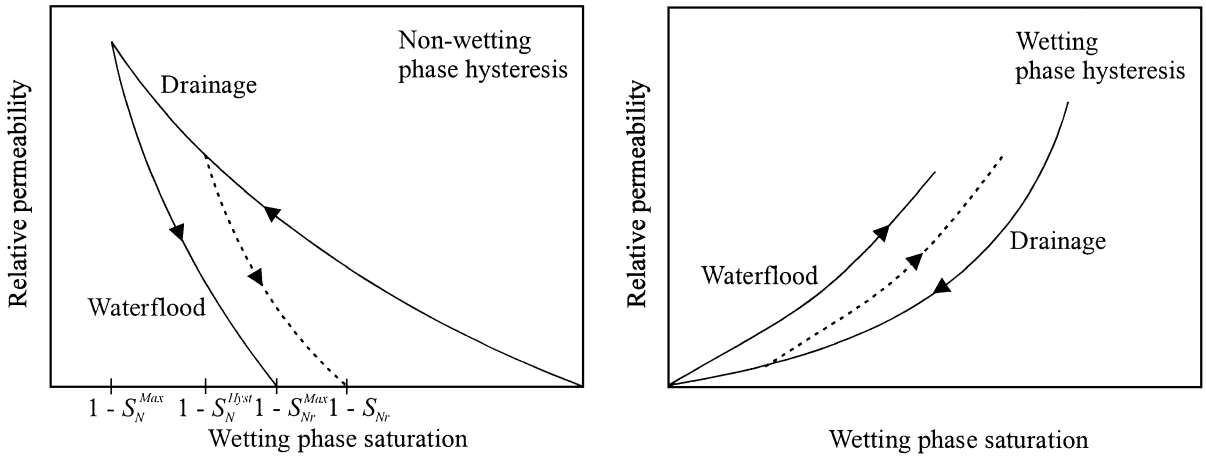

Fig. 6. Hysteresis in relative permeability. Solid lines denote experimentally determined bounding curves; dashed lines denote scanning curves. After Killough (1976). See nomenclature for an explanation of the terms on the left-hand plot.

the scanning curves are obtained by interpolating or re-mapping the bounding curves. Each scanning curve corresponds to a reversal in the direction of saturation change. The first set of scanning curves corresponds to a reversal from drainage to waterflooding, which occurs at the maximum wetting phase saturation obtained after drainage. In a water-wet reservoir, these scanning curves correspond to different initial water saturations. The methods for obtaining the scanning curves are described in Killough (1976) and Carlson (1981) and will not be reproduced here.

5. Comparison of network model and hysteresis model predictions

We now investigate the effect on the waterflood relative permeability curves of varying the water saturation obtained after drainage (the initial water saturation). Our aim was to reproduce the effect of variations in the initial water saturation observed in a transition zone above the OWC. We drained the network to water saturations ranging from connate ($S_{wi} = S_{wc} = 0.25$) to $S_{wi} = 0.9$, and then injected water until all the available pores and throats had been invaded. This yielded a suite of waterflood curves, each of which originates on the drainage curve at a different initial water saturation. For comparison with the hysteresis models of Killough (1976) and Carlson (1981), we assumed that waterflooding from connate water saturation yielded the bounding waterflood curve, which would be measured experimentally.

Initially, we assumed that pores and throats invaded by oil remain water-wet, with the same distribution of advancing contact angles, as used to match the Oak (1990) data (50–80° for all values of S_{wi}; Fig. 7). We then assumed that pores and throats invaded by oil become oil-wet, with the same range of advancing contact angles as used to match the Jadhunandan and Morrow (1995) data (110–180° for all values of S_{wi}; Fig. 8). For convenience, we will refer to this system, in which pores invaded by oil become oil-wet, as generally ‘oil-wet’. In reality, it is likely to vary from oil-wet to mixed-wet becoming less oil-wet as the initial water saturation increases because fewer pores are invaded by oil.

For the water-wet case (Fig. 7), the scanning relative permeability curves lie between the bounding drainage and waterflood curves, as predicted by the hysteresis models of Killough (1976) and Carlson (1981). However, for the oil-wet case, the bounding waterflood curve for water lies above the drainage curve, while the scanning curves lie below the drainage curve (Fig. 8). The bounding curve is measured in the most oil-wet conditions above the transition zone, whereas the scanning curves reflect progressively less oil-wet conditions as the initial water saturation increases and the OWC is approached. For compar-

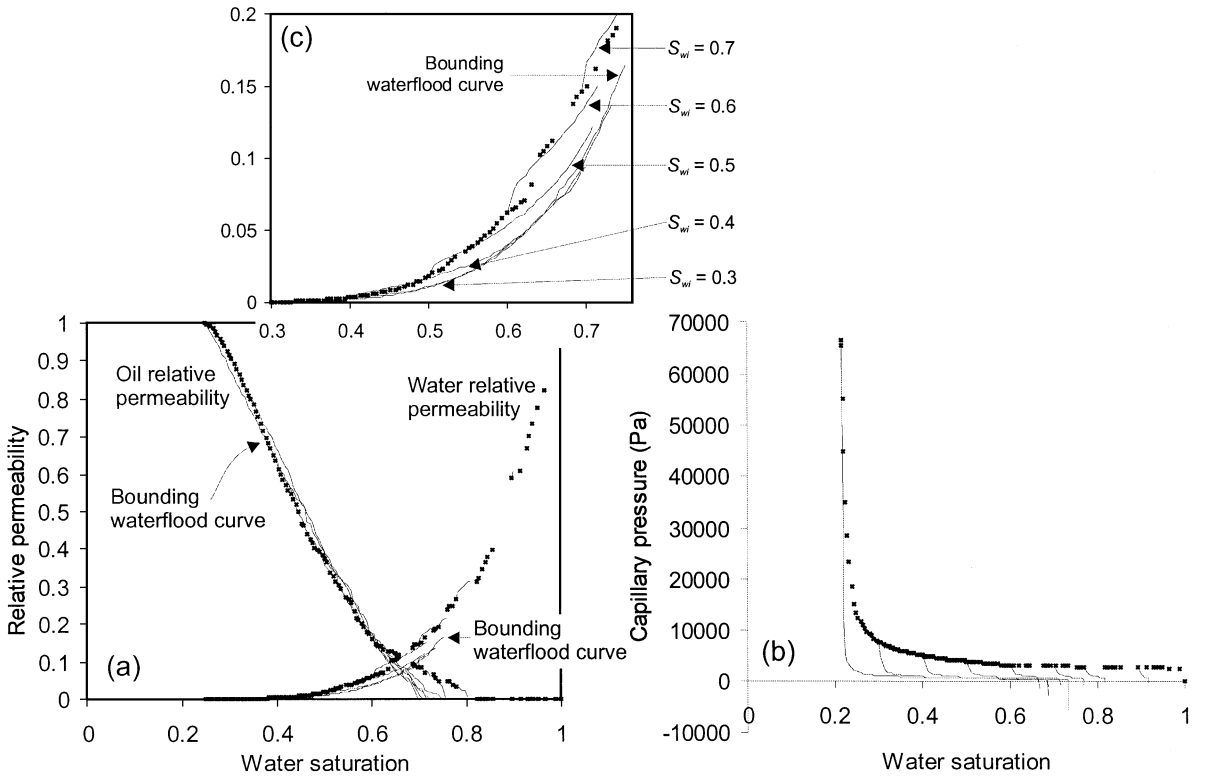

Fig. 7. Relative permeability (a) and capillary pressure (b) curves obtained from the network model. Crosses denote drainage curves, lines denote waterflood (imbibition) curves. The waterflood curves were calculated for initial water saturations ranging from connate ($S_{wi}=S_{wc}=0.25$) to $S_{wi}=0.9$. During waterflooding the advancing contact angle of pores and throats invaded by oil ranged from 50° to 80°. The inset (c) shows a close-up of the water relative permeability curves at small values.

ison, we plot the scanning curves predicted by the Killough model for the bounding drainage and waterflood curves shown in Fig. 8. The results are shown in Fig. 9. The left-hand plot (Fig. 9a) was calculated using the entire waterflood bounding curve. The minimum oil saturation obtained by the network model corresponds to a very small oil relative permeability because oil can continue to flow very slowly through layers (Salathiel, 1973; Zhou et al., 1997). Consequently, the residual oil saturation is much smaller than that which might be measured experimentally or observed in a reservoir following waterflooding. The right-hand plot (Fig. 9b) was therefore obtained using the waterflood bounding curve truncated at a threshold oil relative permeability of 10^{-3}. This is a typical experimental threshold.

Fig. 9 shows that the scanning curves generally lie between the bounding drainage (×) and waterflood (+) curves. The oil scanning curves predicted by the network and empirical models are similar (cf. Figs. 8 and 9). However, the water scanning curves are rather different. Those predicted by the network model are generally lower if they originate at lower initial water saturations, and lie below the bounding drainage curve. Low water relative permeabilities have been measured experimentally in mixed-wet systems (Morrow et al., 1986). Scanning curves predicted by the empirical model generally lie between the bounding drainage and waterflood curves if they originate at lower initial water saturations; however, those which originate at higher initial water saturations fall below the bounding drainage curve, and in this, they are similar to the curves predicted by the network model.

The water relative permeabilities predicted by the network model can be explained by considering the

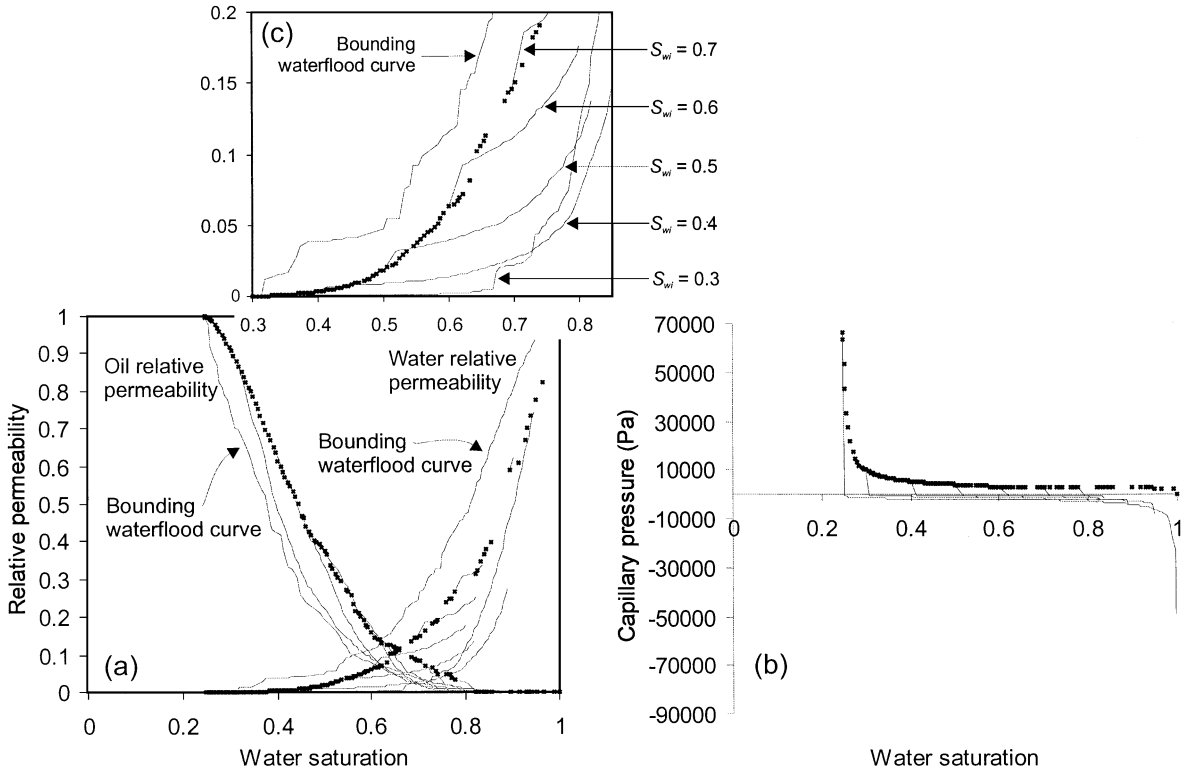

Fig. 8. Relative permeability (a) and capillary pressure (b) curves obtained from the network model. Crosses denote drainage curves, lines denote waterflood curves. The waterflood curves were calculated for initial water saturations ranging from connate ($S_{wi}=S_{wc}=0.25$) to $S_{wi}=0.9$. During waterflooding the advancing contact angle of pores and throats invaded by oil ranged from 110° to 180°. The inset (c) shows a close-up of the water relative permeability curves at small values.

displacement sequence at the pore-scale. During waterflooding, water invades the largest oil-wet pores first. If S_{wi} is close to S_{wc}, waterflooding is essentially a primary drainage type displacement, since almost all the pores and throats are oil-wet (cf. Section 3). The water fills the larger pores and has a high relative permeability. For larger values of S_{wi}, waterflooding is nucleated from many initially water-filled pores, and a large increase in saturation is necessary to form a connected pathway of water-filled pores and throats across the network. Before these pores and throats are connected, k_{rw} is very low as water flow occurs only through wetting layers. As soon as connected water-filled pores and throats span the network, there is a sharp increase in k_{rw} (Fig. 8). This effect is illustrated in Fig. 10 that shows waterflood simulations on a two-dimensional network (simply for ease of visualization) for different values of S_{wi}. The contact angle distribution is the same as in the three-dimensional studies. For $S_{wi}=0$, at $S_w=0.4$, the water forms a path across the model through the centers of the largest pores and throats. Water has entered the network from the inlet and advances in a connected front. This results in a large water relative permeability. For $S_{wi}=0.05$ at the same water saturation, pore filling has occurred throughout the network and water does not span the system through filled pores. The water flow is limited by wetting layers and the corresponding water relative permeability is very low. Note that the S_{wi} values used for the two-dimensional simulations are lower than in the three dimensional simulations, as we have ignored the clay volume.

It is clear that the scanning curves predicted by the network and empirical models are different, which suggests that the empirical models of Killough

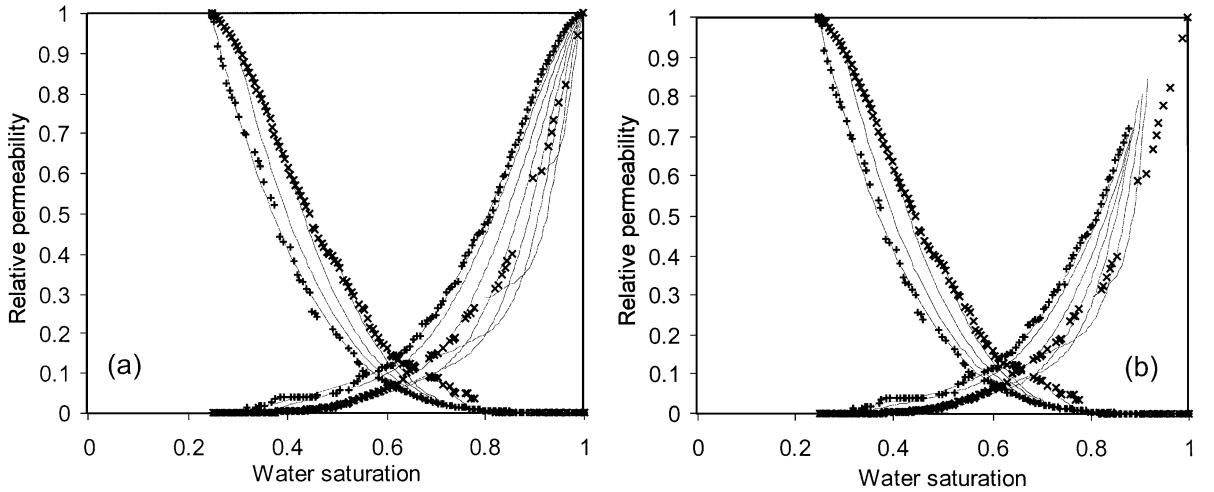

Fig. 9. Scanning curves predicted by the Killough (1976) hysteresis model using the bounding drainage and waterflood curves shown in Fig. 8 for the oil-wet case. The left-hand plot (a) shows scanning curves obtained using the entire waterflood water relative permeability curve. The right-hand plot (b) shows scanning curves obtained using the waterflood water relative permeability curve truncated at an oil relative permeability of 10−3, to mimic the curve which might be measured experimentally. (×) symbols denote drainage bounding curves; (+) symbols denote waterflooding bounding curves (cf. Fig. 8). To generate the scanning curves, best fit curves were matched to the bounding waterflood data.

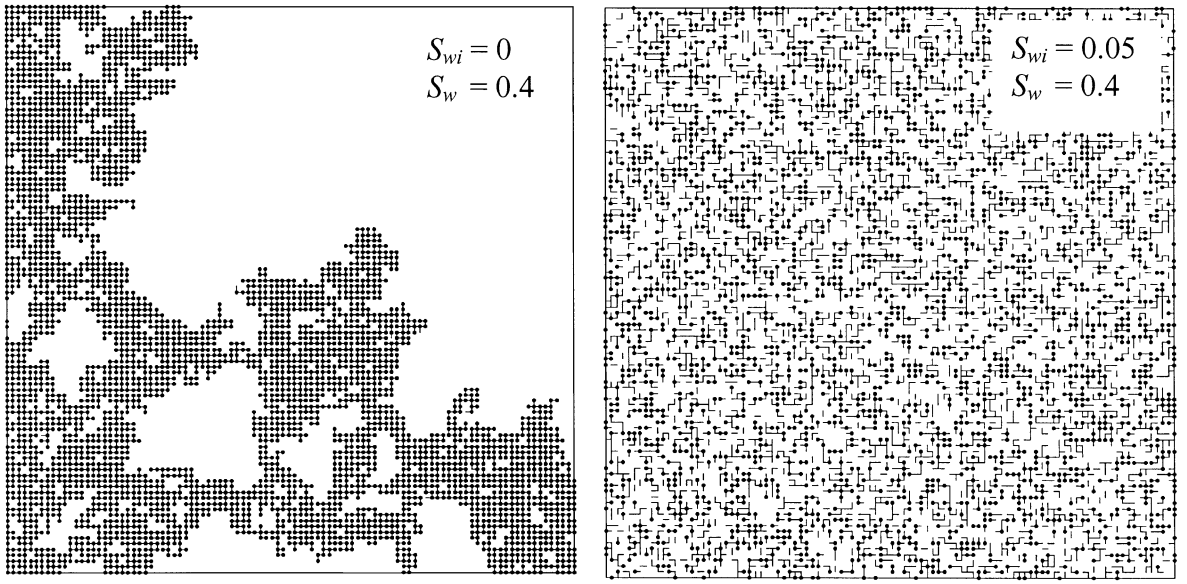

Fig. 10. Two-dimensional simulations of waterflooding at different values of S_{wi} to illustrate the effect of S_{wi} on water connectivity. Pores and throats filled with oil after primary drainage are oil-wet with the same distribution of contact angles used for the three-dimensional network (Fig. 1). For $S_{wi} = 0$ at $S_w = 0.4$ water spans the system. Water invades from the inlet (the left-hand face) as a connected front. In contrast, for $S_{wi} = 0.05$ water filling initiated from originally water-filled pores leads to a more uniform displacement where the water is less well connected. This explains the relative permeabilities in Fig. 8; for a given value of S_w, k_{rw} can decrease as S_{wi} increases.

Table 1
Values of the dimensionless parameters

Aspect ratio	$N_h = h/L$	= 0.075
End-point mobility ratio	$M_e = k^e_{rw}\mu_o/k^e_{ro}\mu_w$	= 0.15 (water-wet) – 1.33 (mixed-wet)
Viscous to gravity ratio	$N_{vg} = \frac{2u_T\mu_o N_h}{\Delta\rho g k k^e_{ro}\cos\theta_d}$	= 0.25
Capillary number	$N_{Pc} = \frac{k^e_{ro}\sigma}{Lu_T\mu_o}\sqrt{\phi k}$	= 0.28

(1976) and Carlson (1981) should not be used to predict hysteresis within a transition zone above the OWC if the wettability varies with height. However, it is not clear whether the differences are significant enough to affect waterflooding at the reservoir-scale. We address this issue in the next section.

6. Effect of hysteresis on waterflooding at the reservoir scale

In this section, we use a conventional simulator in conjunction with the relative permeability and capillary pressure curves obtained from the network model to investigate the reservoir-scale impact of wettability variations on waterflood efficiency. We consider a simple, homogenous, two-dimensional simulation model in which the model volume, fluid mobilities, and balance of forces are described by four dimensionless parameters (Shook et al., 1992; Jackson and Muggeridge, 2000). Their values, which are typical of reservoir-scale displacements, are listed in Table 1. The model is a simple rectangular box with an aspect ratio of 7.5:100, which dips at an angle of $\theta_d = 5°$. The initial distribution of water in the model is dictated by the drainage capillary pressure curve shown in Figs. 7 and 8. The height of the transition zone above the OWC is chosen such that the water saturation falls to connate (S_{wc}) at the top of the model. Simulations are performed on a grid of 250×75 cells; water is injected over the right-hand face of the model, and fluid produced over the left-hand face.

We simulate waterflooding for four different cases: (i) assuming that pores and throats invaded by oil remain water-wet and neglecting hysteresis, using only the bounding waterflood relative permeability curves shown in Fig. 7 (water-wet; no hysteresis); (ii) assuming that pores and throats invaded by oil become oil-wet and neglecting hysteresis, using only the bounding waterflood relative permeability curves shown in Fig. 8 (oil-wet; no hysteresis); (iii) assuming that pores and throats invaded by oil become oil-wet and attempting to include hysteresis by applying the Killough model implemented in Eclipse 100 (Schlumberger Geoquest, 2001), with the bounding drainage and waterflood curves shown

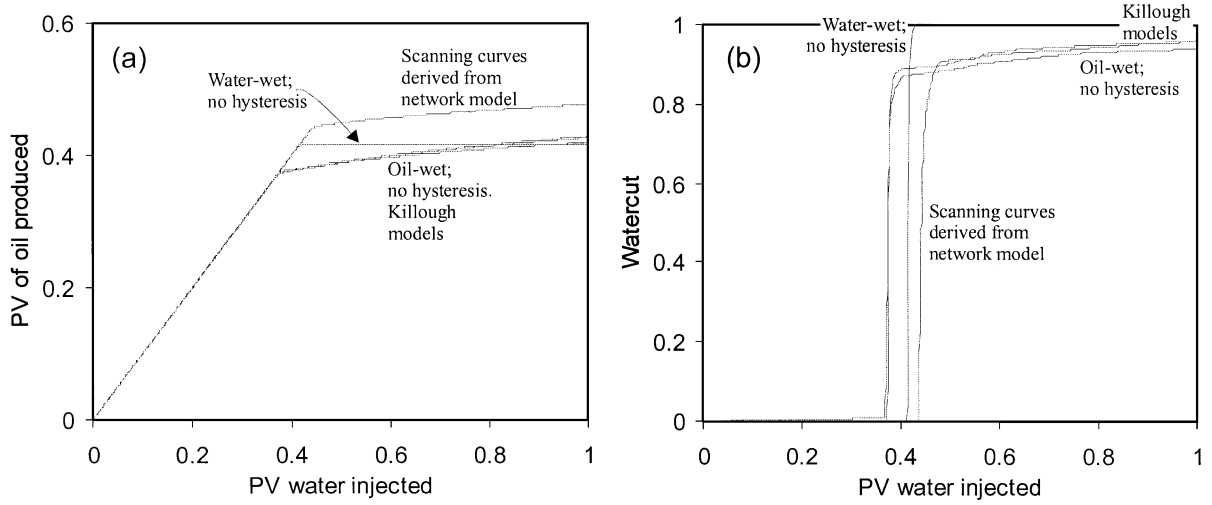

Fig. 11. Pore volumes (PV) of oil produced (a) and watercut (b) as a function of pore volumes of water injected, for each of the simulations run. Oil recovery appears low in terms of rock PV because of the high average initial water saturation within the transition zone.

in Fig. 8. We apply the model both with and without truncation of the bounding curves at an oil relative permeability of 10^{-3} (Killough model with truncation; Killough model without truncation); (iv) assuming that pores and throats invaded by oil become oil-wet and properly including hysteresis by generating a suite of relative permeability curves from the network model, which correspond to the initial water saturations within the simulation model (scanning curves derived from network model). A subset of this suite of curves is shown in Fig. 8. In all simulations, we also include waterflood capillary pressure, either predicted by the network model (e.g. Figs. 7 and 8) or by the Killough model.

The simulations yield the oil produced and water-cut curves shown in Fig. 11, and the water saturation distributions shown in Fig. 12. The results shown in Fig. 11 demonstrate that recovery is significantly higher if hysteresis is properly included using scanning curves generated by the network model. Recovery after 1 PV injected is similar for the other cases regardless of whether the reservoir remains water-

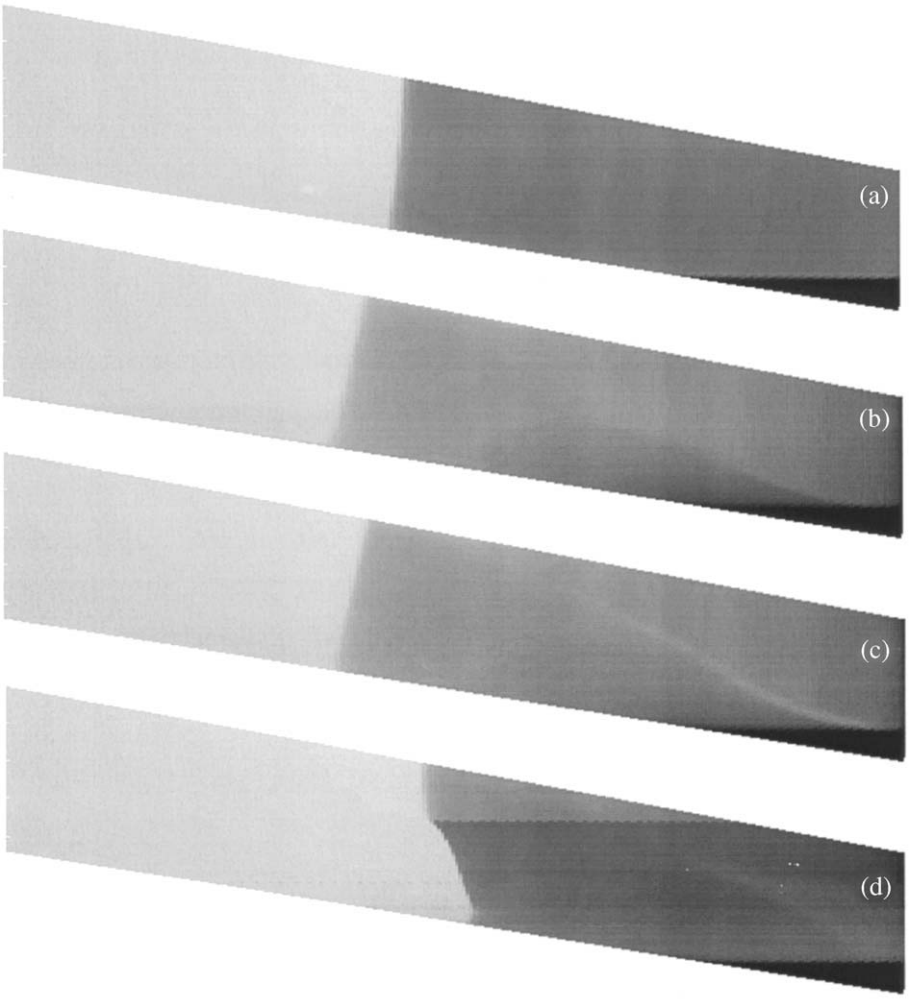

Fig. 12. Water saturation distribution after 0.2 pore volumes of water injected: (a) water-wet; no hysteresis; (b) oil-wet, no hysteresis; (c) Killough model with truncation; (d) scanning curves derived from network model. Dark colours denote high water saturations; vertical exaggeration × 2.

wet or becomes oil-wet and hysteresis is neglected, or whether the reservoir becomes oil-wet and hysteresis is included using the Killough model. Truncating the bounding relative permeability curves at an oil relative permeability of 10^{-3} before applying the Killough model has a negligible effect on either the oil production or the watercut; indeed, production using the Killough models is almost indistinguishable from that obtained using only the oil-wet curves. It would seem that the oil-wet character of the bounding imbibition curves has dominated (Fig. 9). Note that in all cases, oil recovery measured in rock PV appears low due to the high average initial water saturation (~ 0.37) within the transition zone.

Incorporating hysteresis in the oil-wet case by using the network model to generate scanning curves yields a significantly higher recovery after 1 PV injected because the scanning curves display both water-wet and oil-wet characteristics, depending upon the initial water saturation and hence their location within the reservoir. Residual oil saturations are generally much lower than for the water-wet case, yet water relative permeabilities are generally much lower than for the oil-wet case (Fig. 8). This delays water breakthrough and yields a higher oil recovery. The impact of the changing water relative permeabilities with height can be seen in the unusual water saturation distribution (Fig. 12d).

7. Conclusions

We used a three-dimensional pore-scale network representation of a Berea sandstone to investigate relative permeability and capillary pressure hysteresis. We successfully predicted experimental relative permeability data for water-wet Berea sandstone (Oak, 1990), as well as waterflood recoveries for mixed-wet Berea (Jadhunandan and Morrow, 1995). We matched the mixed-wet data reasonably well even when we assumed that wettability variations resulted only from variations in the initial water saturation following primary drainage.

We then studied the effect of variations in initial water saturation associated with capillary rise above the OWC. Relative permeabilities predicted by the network model reflect the pore-scale displacement mechanisms, which are not captured by current empirical hysteresis models. In particular, we predicted that the water relative permeabilities for waterflooding, starting at moderate to high initial water saturations, would be much lower than waterflood curves starting from low initial water saturation.

We then used a conventional simulator in conjunction with the relative permeability curves obtained from the network and empirical models to investigate the reservoir-scale impact of wettability variations on waterflood efficiency. If wettability varies with height above the OWC, we found that using the network model to generate scanning relative permeability curves yields a significantly higher recovery than using empirical scanning curves or assuming uniform wettability. This is because the scanning curves display both water-wet and oil-wet characteristics depending upon the initial water saturation.

Our results suggest that the proper inclusion of hysteresis is important to predict recovery if wettability varies with height above the OWC. Assuming that the reservoir is uniformly water-wet or oil-wet, or using an empirical hysteresis model, may lead to an underestimate of recovery.

Nomenclature

g	gravitational acceleration, L t^{-2}, m s^{-2}
h	height of model volume, L, m
h_t	height of transition zone, L, m
k	permeability L^2, m^2
k_{ro}	oil relative permeability
k_{rw}	water relative permeability
k_{ro}^e	oil end-point relative permeability
k_{rw}^e	water end-point relative permeability
L	length of model volume, L, m
M_e	end-point mobility ratio
n	number of surrounding throats filled with oil
N_{vg}	viscous-to-gravity ratio
N_h	height number (aspect ratio)
N_{Pc}	capillary number
P_c^{max}	maximum capillary pressure, m L^{-1} t^{-2}, Pa
P_{cap}	capillary entry pressure, m L^{-1} t^{-2}, Pa
r	pore radius, L, m
S_{Nr}	residual non-wetting phase saturation
S_N^{Hyst}	maximum non-wetting phase saturation for given scanning curve
S_{Nr}^{Max}	maximum residual non-wetting phase saturation

S_N^{Max}	maximum non-wetting phase saturation
S_{wc}	connate water saturation
S_{wi}	initial water saturation
S_{or}	residual oil saturation
u_T	total flow velocity, L t^{-1}, m s^{-1}
γ	interfacial tension, mL t^{-2}, mN m^{-1}
μ_o	oil viscosity, m L^{-1} t^{-1}, Pa s
μ_w	water viscosity, m L^{-1} t^{-1}, Pa s
θ_a	advancing contact angle, °
θ_r	receding contact angle, °
θ_d	dip of model, °
$\Delta\rho$	water-oil density contrast, m L^{-3}, kg m^{-3}

Acknowledgements

The members of the Imperial College consortium on Pore-Scale Modelling (BHP, Enterprise Oil, Gaz de France, JNOC, PDVSA-Intevep, Schlumberger, Shell, Statoil, the U.K. Department of Trade and Industry and the EPSRC) are thanked for their financial support. We also thank Pål-Eric Øren (Statoil) for sharing his Berea network data with us.

References

Anderson, W.G., 1987. Wettability literature survey—Part 5: the effects of wettability on relative permeability. J. Pet. Technol., 1453–1468 (November).

Bakke, S., Øren, P.E., 1997. 3-D pore-scale modelling of sandstones and flow simulations in the pore networks. Soc. Pet. Eng. J. 2, 136.

Blunt, M.J., 1997a. Effects of heterogeneity and wetting on relative permeability using pore-level modelling. Soc. Pet. Eng. J. 2, 70–87.

Blunt, M.J., 1997b. Pore level modelling of the effects of wettability. Soc. Pet. Eng. J. 2, 449–510.

Blunt, M.J., 1998. Physically-based network modelling of multiphase flow in intermediate-wet porous media. J. Pet. Sci. Eng. 20, 117–125.

Blunt, M.J., Jackson, M.D., Piri, M., Valvatne, P.H., 2002. Detailed physics, predictive capabilities and upscaling for pore-scale models of multiphase flow. Adv. in Water Res. 25, 1069–1089.

Buckley, J.S., 1995. Asphaltene precipitation and crude oil wetting. Soc. Pet. Eng. Adv. Technol. Ser. 3, 53.

Buckley, J.S., Liu, Y., 1998. Some mechanisms of crude oil/brine/solid interactions. J. Pet. Sci. Eng. 20, 155–160.

Buckley, J.S., Takamura, K., Morrow, N.R., 1989. Influence of electrical surface charges on the wetting properties of crude oils. Soc. Pet. Eng. Form. Eval. 4, 240–332.

Buckley, J.S., Bousseau, C., Liu, Y., 1996. Wetting alteration by brine and crude oil: from contact angles to cores. Soc. Pet. Eng. J. 1, 341–350.

Carlson, F.M., 1981. Simulation of relative permeability hysteresis to the non-wetting phase. SPE paper 10157. Proceedings of the Annual Technical Conference and Exhibition, San Antonio, 5–7 Oct.

Craig, F.F., 1971. The reservoir engineering aspects of waterflooding. Monograph Series. SPE, Richardson, TX.

Dias, M.M., Wilkinson, D., 1986. Percolation with trapping. J. Phys. A: Math Gen. 19, 3131–3146.

Dixit, A.S., McDougall, S.R., Sorbie, K.S., 1997. A pore-level investigation of relative permeability hysteresis in water-wet systems. SPE paper 37233. Proceedings of the SPE International Symposium on Oilfield Chemistry, Houston, 18–21 Feb.

Dixit, A.S., McDougall, S.R., Sorbie, K.S., 1998. Analysis of relative permeability hysteresis trends in mixed-wet porous media using network models. SPE paper 39656. Proceedings of the SPE/DOE Improved Oil Recovery Symposium, Tulsa, 19–22 April.

Dixit, A.S., McDougall, S.R., Sorbie, K.S., Buckley, J.S., 1999. Pore-scale modelling of wettability effects and their influence on oil recovery. Soc. Pet. Eng. Res. Eval. Eng. 2, 25–36.

Dubey, S.T., Doe, P.H., 1993. Base number and wetting properties of crude oils. Soc. Pet. Eng. Res. Eng. 8, 195.

Dubey, S.T., Waxman, M.H., 1991. Asphaltene adsorption and desorption from mineral surfaces. Soc. Pet. Eng. Res. Eng. 6, 389.

Firincioglu, T., Blunt, M.J., Zhou, D., 1999. Three-phase flow and wettability effects in triangular capillaries. Colloids Surf., A 155, 259–276.

Hamon, G., 2000. Field-wide variations of wettability. SPE paper 63144. Proceedings of the SPE Annual Technological Conference and Exhibition, Dallas, Texas, 1–4 Oct.

Hazlett, R.D., 1990. Fractal applications: wettability and contact angle. J. Colloid Interface Sci. 137, 527–533.

Heiba, A.A., Davis, H.T., Scriven, L.E., 1983. Effect of wettability on two-phase relative permeability and capillary pressures. SPE paper 12172. Proceedings of the SPE Annual Technological Conference and Exhibition, San Francisco, 5–8 Oct.

Hilfer, R., Øren, P.E., 1996. Dimensional analysis of pore scale and field scale immiscible displacement. Transp. Porous Media 22, 53.

Hirasaki, G.J., 1991. Wettability: fundamentals and surface forces. Soc. Pet. Eng. Form. Eval. 6, 217–226.

Hui, M.H., Blunt, M.J., 2000. Effects of wettability on three-phase flow in porous media. J. Phys. Chem., B 104, 3833–3845.

Jackson, M.D., Muggeridge, A.H., 2000. Effect of discontinuous shales on reservoir performance during horizontal waterflooding. Soc. Pet. Eng. J. 5, 446–455.

Jadhunandan, P.P., Morrow, N., 1995. Effect of wettability on waterflood recovery for crude-oil/brine/rock systems. Soc. Pet. Eng. Res. Eng. 10, 40–46.

Jerauld, G.R., 1996a. Gas–oil relative permeability of prudhoe bay. SPE paper 35718. Proceedings of the SPE Western Regional Meeting, Anchorage, Alaska, 22–24 May.

Jerauld, G.R., 1996b. General three-phase relative permeability

model for Prudhoe Bay. SPE paper 36178. Proceedings of the 7th ADIPEC Meeting, Abu Dhabi, 13–16 Oct.

Jerauld, G.R., Rathmell, J.J., 1997. Wettability and relative permeability of prudhoe bay: a case study in mixed-wet reservoirs. Soc. Pet. Eng. Res. Eng. 12, 58–65.

Killough, J.E., 1976. Reservoir simulation with history-dependent saturation functions. Soc. Pet. Eng. J. 16, 37–48.

Kossack, C.A., 2000. Comparison of reservoir simulation hysteresis options. SPE paper 63147. Proceedings of the Annual Technical Conference and Exhibition, Dallas, 1–4 Oct.

Kovscek, A.R., Wong, H., Radke, C.J., 1993. A pore-level scenario for the development of mixed wettability in oil reservoirs. AIChE J. 39, 1072–1085.

Land, C.S., 1968. The optimum gas saturation for maximum oil recovery from displacement by water. SPE paper 2216. Proceedings of the Annual Technical Conference and Exhibition, Houston, 29 Sept.–2 Oct.

Lenormand, R., Zarcone, C., 1984. Role of roughness and edges during imbibition in square capillaries. SPE paper 13264. Proceedings of SPE Annual Technological Conference and Exhibition, Houston, 16–19 Sept.

Lenormand, R., Touboul, E., Zarcone, C., 1988. Numerical models and experiments on immiscible displacements in porous media. J. Fluid Mech. 189, 165–187.

McDougall, S.R., Sorbie, K.S., 1995. The impact of wettability on waterflooding: pore scale simulation. Soc. Pet. Eng. Res. Eng. 10, 208.

Mohanty, K.K., Salter, S.J., 1983. Multiphase flow in porous media: part 3-oil mobilization, transverse dispersion and wettability. Paper SPE 12127. Proceedings of the SPE Annual Technological Conference and Exhibition, San Francisco, 5–8 Oct.

Morrow, N.R., 1990. Wettability and its effect on oil recovery. J. Pet. Technol., 1476–1484 (December).

Morrow, N.R., Lim, H.T., Ward, J.S., 1986. Effect of crude-oil-induced wettability changes on oil recovery. Soc. Pet. Eng. Form. Eval. 1, 89–103.

Oak, M.J., 1990. Three-phase relative permeability of water-wet berea. SPE paper 20183. Proceedings of the SPE/DOE Enhanced Oil Recovery Symposium, Tulsa, Oklahoma, 22–25 April.

Onda, T., Shibuichi, S., Satoh, N., Tsujii, K., 1996. Super-water-repellant fractal surfaces. Langmuir 12, 2125–2127.

Øren, P.E., Bakke, S., 2002. Process base reconstruction of sandstones and prediction of transport properties. Transp. Porous Media 46, 311–343.

Øren, P.E., Bakke, S., Arntzen, O.J., 1998. Extending predictive capabilities to network models. Soc. Pet. Eng. J. 3, 324–336.

Owens, W.W., Archer, D.L., 1971. The effect of rock wettability on oil–water relative permeability relationships. J. Pet. Technol., 873–878 (July).

Patzek, T.W., 2001. Verification of a complete pore network simulator of drainage and imbibition. Soc. Pet. Eng. J. 6, 144–156.

Salathiel, R.A., 1973. Oil recovery by surface film drainage in mixed wettability rocks. J. Pet. Technol., 1216–1224 (October).

Schlumberger Geoquest, 2001. Eclipse 100 Reference Manual, Schlumberger Geoquest.

Shook, M., Li, D., Lake, L.W., 1992. Scaling immiscible flow through porous media by inspectional analysis. In Situ 16, 311–349.

Wilkinson, D., Williamsen, J.F., 1983. Invasion percolation: a new form of percolation theory. J. Phys. A: Math Gen. 16, 3365–3376.

Wolcott, J.M., Groves Jr., F.R., Lee, H.G., 1993. Investigation of crude-oil/mineral interactions: influence of oil chemistry on wettability alteration. SPE paper 25194. Proceedings of the SPE International Symposium of Oil Field Chemistry, New Orleans, 2–5 Mar.

Zhou, D., Blunt, M., Orr Jr., F.M., 1997. Hydrocarbon drainage along corners of noncircular capillaries. J. Colloid Interface Sci. 187, 11–21.

Zhou, X., Morrow, N.R., Ma, S., 2000. Interrelationship of wettability, initial water saturation, aging time and oil recovery by spontaneous imbibition and waterflooding. Soc. Pet. Eng. J. 5, 199–207.